ELSEVIER

19 May 1995

Chemical Physics Letters 237 (1995) 525-535

CHEMICAL PHYSICS LETTERS

Resonance in the dynamics of chemical systems simulated by the implicit midpoint scheme

Margaret Mandziuk, Tamar Schlick

The Howard Hughes Medical Institute and New York University, Chemistry Department and Courant Institute of Mathematical Sciences, 251 Mercer Street, New York, NY 10012, USA [1]

Received 24 December 1994; in final form 7 March 1995

Abstract

The numerical behavior of the symplectic, implicit midpoint method with a wide range of integration timesteps is examined through an application to a diatomic molecule governed by a Morse potential. Our oscillator with a 12.6 fs period exhibits notable, integrator induced, timestep- (Δt) dependent resonances and we predict approximate values of Δt where they will occur. The particular case of a third-order resonance ($\Delta t \approx 7$ fs here) leads to instability, and higher-order resonances ($n = 4, 5$) to large energetic fluctuations and/or corrupted phase diagrams. Significantly, for $\Delta t > 10$ fs the energy errors remain bound.

1. Introduction

In molecular dynamics (MD) simulations of biomolecules, complex motion is followed by numerically integrating Newton's classical equations

$$\mathbf{M}\dot{V}(t) = f(X), \tag{1}$$

$$\dot{X}(t) = V(t), \tag{2}$$

where $\mathbf{M}$ is a mass matrix, X is the collective Cartesian vector of positions, V is the corresponding collective velocity vector, f is the effective force vector, and the dot superscripts denote differentiation with respect to time, t. Because the underlying forces are nonlinear and the multivariate potential energy landscape very complex – rich with minima, maxima and transition points – simulating these systems in time by computer presents a formidable task. The challenge arises not only from the size (thousand of variables) and nonlinearity of the governing equations but also from the timescales of biological interest that must be followed. The collective modes in biological molecules such as proteins, DNA, and RNA are several orders of magnitude slower than the high-frequency vibrational modes [1]. Moreover, the amplitudes of displacements associated with the low frequencies are much greater than those of the high frequencies and therefore crucial for biological activity. Examples of such large displacements include internal conformational rearrangements, enzymatic reactions, and protein folding. Computer models offer an important tool for studying these problems which are far from being resolved in the experimental laboratory.

In practice, this disparity of timescales in biomolecules imposes a severe restriction on the integration timestep (Δt) for numerical stability considerations: Δt must be a fraction of the fastest period, which is around 10^{-14} s for a C–H stretch [2,3]. With

[1] Internet: schlick@nyu.edu

SSDI 0009-2614(95)00316-9

such a small time increment, the fastest computers today can only produce biomolecular trajectories on the nanosecond scale, still several orders away from the processes of major interest, as outlined above. It is far from clear that much longer simulations alone will be successful at unveiling many processes that elude us today, as there are also serious approximations in the governing force field, as well as the underlying thermodynamic assumption (i.e. unmediated folding). Nonetheless, devising new strategies for increasing the feasible timestep – and hence the simulation times – forms an exciting area of research, not only for biophysics but also for applied mathematics, since new and complex problems emerge for which no standard mathematical body is entirely suitable.

Implicit numerical integrators have been widely known to the mathematical community as methods with high stability for problems of multiple timescales [4]. They have also been introduced to molecular dynamics simulations [5,6], but straightforward application, even with random forces (in the context of Langevin dynamics) to counteract numerical dissipation, can lead to uncompensated damping, which in turn alters chemical dynamics. Thus, their use has been recommended in combination with other procedures that properly resolve the system's subdynamics [3,7], or for macroscopic models where the high frequency modes are absent by construction [8,9]. In any case, implicit integrators are clearly computationally demanding since solution of a nonlinear system of equations is involved at every dynamical step. Nonetheless, minimization formulations of this additional task and procedures to accelerate minimization convergence [5,6,10] through preconditioning and clever initial guesses can make these methods feasible, if not competitive.

Symplectic numerical integrators for Hamiltonian systems have gained favorable attention in recent years [11–13]. Symplecticness is a highly desirable property associated with dynamical systems that leads to preservation of areas in phase space and ensures long-time stability of the method [12]. One symplectic scheme is implicit midpoint (IM). In the linear regime, the energy is known to be conserved and stability to hold at large timesteps [12]. However, certain associated problems in the nonlinear regime, namely of resonance and large energetic fluctuations at large timesteps [14,15], have limited IM applications to biomolecules.

Recent numerical results of Simo et al. [16,17] indicate that symplectic algorithms introduce artificial coupling among the motions associated with various frequencies, leading to instability. Chaotic behavior, exhibited by symplectic integrators, for one-dimensional nonlinear Hamiltonian systems (theoretically integrable and non-chaotic), were also reported [14,18]! Thus, it is of particular interest (and concern) to explore how IM will behave for naturally chaotic systems, such as biomolecules.

It is the purpose of this work to begin a feasibility study regarding IM applications to chemical systems at large timesteps. We are not interested here in very accurate trajectories, such as can only be obtained with high-order methods and small timesteps with respect to the highest frequency of the motion. Rather, our goal is to approximate reasonably, in some way, the natural features of our physical systems so that long-time processes can be followed to generate new biological insight. Clearly, one expects errors when the timestep is not sufficiently small to resolve the highest frequency, especially with a low-order integrator (e.g., one or two). However, it is of interest to distinguish between systematic errors that increase with the timestep and more erratic ones, such as caused by resonance. Moreover, explaining the origin and effects of those resonances might aid in developing remedies for these serious artificial effects. Thus, the following questions form the main focus of this Letter:

(1) How large can the timestep be in IM to yield similar energetic fluctuations as observed with standard explicit simulations at small timesteps (e.g., Δt = 1 fs)?

(2) How does IM perform as Δt increases and what are possible problems?

(3) What might explain those problems? Are they predictable?

(4) What can be concluded about the prospects of IM for biomolecular dynamics?

Computational issues (i.e. competitiveness of the scheme with respect to small-timestep explicit schemes) can only be addressed through applications to a wide range of system types and sizes. However, CPU issues will be relevant only if reliable, or at least predictable, performance can be ensured.

2. Model and method

2.1. Propagation schemes (IM and Verlet)

The IM scheme, applied to the Newtonian equations of motion (Eqs. (1) and (2)), is described by the discretization

$$\frac{V^{n+1}-V^n}{\Delta t} = \mathbf{M}^{-1} f(\tfrac{1}{2}(X^n + X^{n+1})), \tag{3}$$

$$\frac{X^{n+1}-X^n}{\Delta t} = \tfrac{1}{2}(V^n + V^{n+1}). \tag{4}$$

The superscripts n denote the difference-equations solution to X at time $n\Delta t$, and $f = -\nabla E_p$, the gradient of the potential energy E_p. Following Ref. [5], the new position vector, X^{n+1}, can be calculated by minimizing the 'dynamics' function, $\Phi(X)$, which for IM takes form

$$\Phi(X) = \tfrac{1}{2}(X - X_0^n)\,\mathbf{M}\,(X - X_0^n) + (\Delta t)^2 E_p(\tfrac{1}{2}(X + X^n)), \tag{5}$$

with

$$X_0^n = X^n + \Delta t V^n. \tag{6}$$

To begin a trajectory with IM, only X^0 and V^0 must be specified. The minimization procedure is performed with the truncated-Newton minimization package, TNPACK [19,20]. This makes implicit integrators feasible for biomolecules. Here, the initial guess for Φ minimization is taken as X^n. Once X^{n+1} is computed, V^{n+1} is calculated directly from the relation given in Eq. (4).

For comparison, we also propagate the motion of the Morse oscillator with the commonly used Verlet algorithm [21], whose updating formula is given by

$$X^{n+1} = 2X^n - X^{n-1} + (\Delta t)^2 f(X^n). \tag{7}$$

The velocity, not necessary for the position propagation, can be defined as

$$V^n = \frac{X^{n+1} - X^{n-1}}{2\Delta t}. \tag{8}$$

The propagation of positions according to Eq. (7) requires initial specification of both X^0 and X^1. When X^1 is set to

$$X^1 = X^0 + \Delta t V^0 + \tfrac{1}{2}\Delta t^2 f(X^0), \tag{9}$$

the scheme is equivalent to the leap-frog method [22], known to be symplectic [23]. Here, we choose initial conditions according to the above equation, so the leap-frog method is tested.

2.2. Morse potential parameters

Our model system is the diatomic molecule, HBr, with the hydrogen and bromine atoms interacting via the Morse potential [24]

$$E_p(r) = D\{1 - \exp[-S(r - r_0)]\}^2. \tag{10}$$

In the above equation, r represents the interatomic distance, ($r = ||x_H - x_{Br}||$ with x_H and x_{Br} denoting position vectors of the hydrogen and bromine atoms, respectively); D is the well depth, S is a parameter controlling the width of the well, and r_0 is the equilibrium bond distance. The potential parameters for HBr follow those used in Ref. [6]. Specifically, D = 90.5 kcal/mol, S = 1.814 Å^{-1}, and r_0 = 1.41 Å. The masses of hydrogen and bromine are set to m_H = 1.00785 amu, and m_{Br} = 79.904 amu, respectively. The resulting reduced mass, $\mu = m_H m_{Br}/(m_H + m_{Br})$, is then 0.9953 amu.

To study the effect of the IM discretization on the Morse potential alone, we restrict our application to a diatomic molecule moving in one dimension under the influence of this potential. (In practice, a 3D model is simulated with zero initial conditions for X and V in two of the three components to eliminate rotation; the kinetic energy resulting from translation of the free coordinate is then subtracted.) The conjugate pair of position and momentum for the Morse oscillator alone (r, p), is then expressed in terms of two nuclear positions (x_H and x_{Br}) and the two velocities (v_H and v_{Br}) of the hydrogen and bromine atoms as follows:

$$r = x_{Br} - x_H, \tag{11a}$$

$$p = \mu(v_{Br} - v_H). \tag{11b}$$

The phase diagrams shown in this Letter display the magnitude of r, r, and the x component of p, p (y and z components of p are zero). The Morse oscillator represents a simple nonlinear system on which numerical procedures can readily and systematically be tested. Moreover, exact trajectories are known analytically [24]. They are expressed in terms of an energy-

dependent angular frequency, ω_{E_t}, which is given by the formula

$$\omega_{E_t} = S\sqrt{\frac{2(D - E_t)}{\mu}}. \qquad (12)$$

Here, E_t represents total energy of the system.

3. Results

Results for IM are analyzed below by examining behavior of the energies and phase spaces by two procedures: (1) varying Δt but fixing initial conditions, and (2) fixing Δt but changing the initial conditions. Both procedures provide insight into the behavior of the system, particularly near chaotic or problematic regions.

The initial conditions for calculations with varying timestep are chosen to mimic those typically used in MD simulations. The initial position was taken as an average position for desired temperature of the system, and the initial velocity was set according to the target temperature. In our calculations, the temperature is chosen to be around 600 K. (At that temperature the nonlinear effects are stronger that at room temperature, while the total energy is still low relative to dissociation energy.) Initial conditions are specified as follows: $x_H^0 = (1.4155, 0, 0)^\top$ Å, $v_H^0 = (1.545, 0, 0)^\top$ Å/τ, $x_{Br}^0 = (0, 0, 0)^\top$ Å, $v_{Br}^0 = (0, 0, 0)^\top$ Å/τ, where τ is a time unit used in our calculations, corresponding to 48.888 fs [6]. The total energy (kinetic plus potential) of the Morse oscillator (not including translational energy), at this set of initial conditions is $E_t^0 = E_k^0 + E_p^0 = 1.197$ kcal/mol. The corresponding angular frequency of the periodic motion at that value of energy, calculated from Eq. (12), is $\omega_{E_t^0} = 0.4970$ fs^{-1} with the period $T_{E_t^0} = 12.6$ fs.

As reported already [12], propagation of a nonlinear system with IM does not preserve the value of the total energy from step to step. Instead, fluctuations are expected, with their magnitude depending on the timestep. Figs. 1a–1c shows the average values of the total energy, $\langle E_t \rangle$, versus Δt, as well as the magnitude of fluctuations of the total energy (minimum and the maximum values of E_t), obtained along the trajectories simulated by both IM and the leap-frog schemes. Data were collected by averaging the total energy, E_t, over 20000 to 100000 steps (more steps near resonances and/or large values of Δt), so as to ensure a converged value to at least three significant figures.

A striking pattern emerges. For small timesteps, the computed values of total energy are in very good agreement with the exact value, E_t^0. Moreover, for timesteps in the range up to 2 fs (roughly, one sixth of the period), the fluctuations of IM are much smaller than those obtained with the explicit integrator (Fig. 1c), by an order of magnitude for $\Delta t = 2$ fs. Now, with increasing Δt, the range of fluctuations in IM systematically increases, as in leap-frog. However, for timesteps around 4 and 7 fs (approximately one third and one half of the period), the fluctuations in IM increase dramatically, leading to instability for $\Delta t \approx 7$ fs. Nonetheless, further increase of the timestep leads to a bounded range of fluctuations, converging to a finite value, as shown for $\Delta t > 10$ fs. As will be shown below, at large timesteps the frequency of the system is altered (Fig. 1d).

In Fig. 2 we show the IM kinetic, potential and total energy distributions as well as phase space diagrams, for selected timesteps. For $\Delta t = 1$ fs (Fig. 2a), the phase diagram of the simulated trajectory lies very close to the analytical one and, within the resolution of the plot, they overlap. Correspondingly, the fluctuations of the energy are very small from the starting value. The kinetic and potential energy distributions appear as mirror images: the potential energy has a minimum at r_0, while E_k has a maximum, and as one component increases the other decreases correspondingly. When the timestep is increased to $\Delta t = 2$ fs (Fig. 2b), the simulated trajectory slightly, but visibly, differs from the exact one, resulting in larger fluctuations of the total energy.

The timestep in Fig. 2c ($\Delta t = 4.02$ fs) corresponds to the region for which large energy fluctuations are noted in Fig. 1. Although the average total energy $\langle E_t \rangle = 1.37$ kcal/mol is within the 20% of E_t^0, the sampled trajectory is qualitatively different from the analytical one for the Morse oscillator: It reveals four separate islands. Now, in addition to stretched bond-length values, r, the absolute value of momentum, $|p|$ (x direction), can take two different values for a given value of r; thus, the kinetic energy distribution is doubly valued. This in turn causes a highly inaccurate, doubly valued pattern of the total energy distribution. The next two parts of Figs. 2d and 2e are chosen

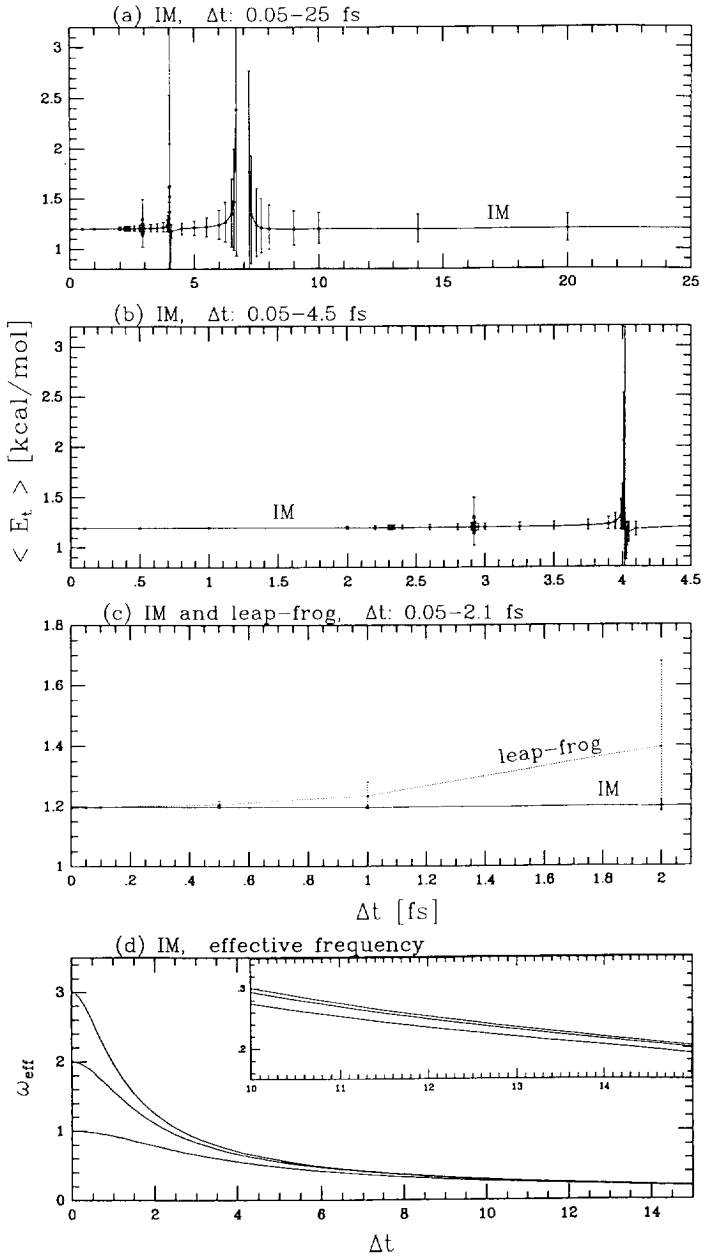

Fig. 1. The total energy envelopes (kinetic plus potential), obtained for the HBr Morse system by explicit (leap-frog) and implicit midpoint (IM) integration (a)–(c); and the effective angular frequency of the harmonic oscillator, ω_0^{eff}, defined by Eq. (18) (d). Average energies and associated envelopes (indicating fluctuation ranges) are calculated from trajectories that cover 20000 to 100000 steps to ensure that the average energy converges to at least three significant figures. Whereas the size of envelopes and the mean energy values increase steadily with the timestep (Δt) for leap-frog, behavior of IM, though very good for $\Delta t < 2$ fs in comparison to leap-frog, indicates resonance problems at particular timesteps (e.g., $\Delta t = 2.9, 4.02, 7$ fs). Significantly, beyond $\Delta t = 10$ fs, the errors in the IM envelopes are bound. The three curves in (d) correspond to different original frequencies of the harmonic oscillator, namely $\omega_0 = 1, 2, 3$ rad.

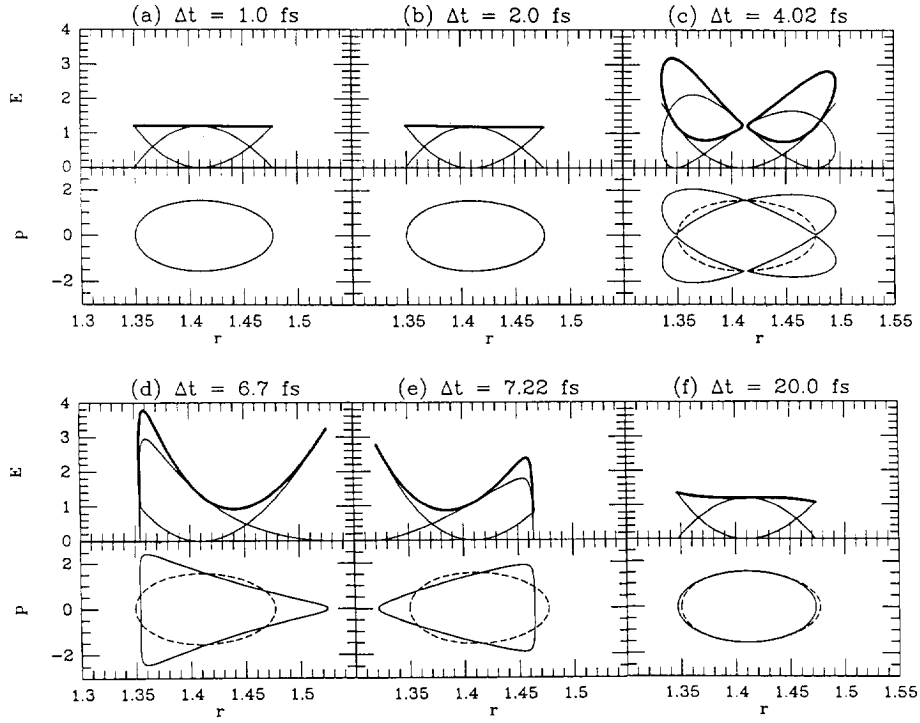

Fig. 2. Energy distributions (kinetic, potential and total) and phase diagrams obtained for IM trajectories at various timesteps. For the timesteps $\Delta t = 1.0, 2.0, 4.02, 6.7, 7.22, 20.0$ fs, we show the energy (E) *distributions* as a function of the bond length (r), along with the corresponding phase diagram (r, p, see Eqs. (11a) and (11b)). For each timestep, the distribution for the total energy are shown as dark lines. The curve of potential energy distribution can be identified by a characteristic minimum at r_0. The remaining curve represent the kinetic energy distribution. The analytical trajectory is shown as a dashed line on the phase plot for comparison with the simulated one. The regular symmetric pattern at small timesteps is quickly replaced by more intricate energy patterns, indicating the selective sampling of phase space. Here and in all other phase diagrams, r is given in Å, p in amu Å/τ, and energy in kcal/mol (τ is the time unit used in our calculations corresponding to 48.888 fs [6]).

for timesteps slightly lower ($\Delta t = 6.7$ fs) and higher ($\Delta t = 7.22$ fs) than that associated with the instability region. For these IM trajectories, the sampling of the phase space is incorrect: trajectories are triangularly shaped. Extended values of r and p are covered and large energy fluctuations result. Notice that the triangularly shaped phase diagrams of Figs. 2d and 2e appear to be rotated by π relative to each other. The plots presented in Fig. 2f are obtained with $\Delta t = 20$ fs. As shown in Fig. 1a, for large timesteps ($\Delta t > 10$ fs), $\langle E_t \rangle$ is nearly constant and fluctuations are bound. The sampled trajectory for that timestep resembles the one for a harmonic oscillator centered at r_0 (initial point (r^0, p^0) is contained in it), since the force is essentially linearized. The computed average value of the bond length for that timestep is $\langle r \rangle = 1.4102$ Å (1.4155 Å for $\Delta t = 1$ fs). For $\Delta t > 20$ fs phase space maps are very similar to that one presented in Fig. 2f (data not shown). Also, $\langle r \rangle \rightarrow r_0$ as $\Delta t \rightarrow \infty$, indicating that in the limit of large timesteps, the trajectory approaches that of a harmonic oscillator. The effective sampling of the linearized system explains the boundedness of the energy fluctuations. Recall that harmonic oscillator orbits obtained by IM are identical for any timestep. Thus for large timesteps the average values of the total energy and energetic fluctuations depend largely on the initial conditions, not on the timestep (within reasonable accuracy).

In Fig. 3 (color plate) we show phase diagrams of the trajectories obtained with several Δt values near the 'resonance' of 2.9 fs (about one fourth of the period). All of these trajectories begin at the same initial point, as described above, and each trajectory contains at least 5000 successive points from the simulation.

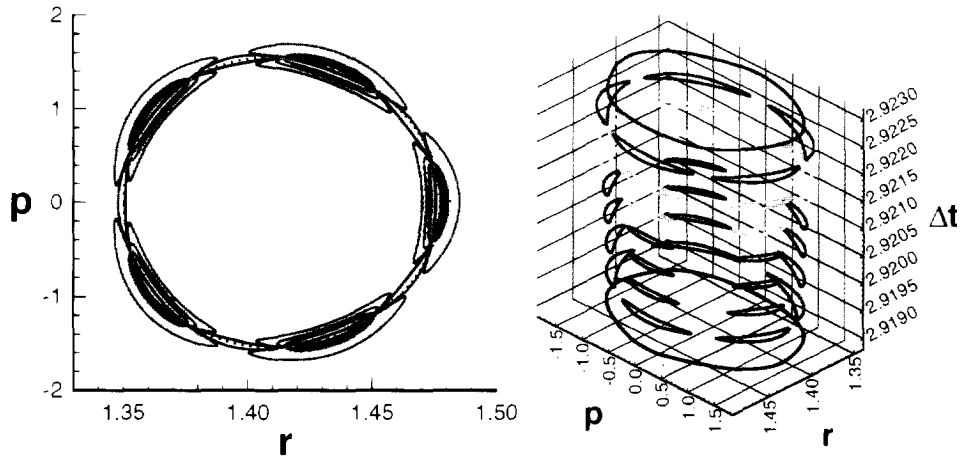

Fig. 3. IM phase diagrams for the Morse oscillator corresponding to fixed initial conditions at different timesteps near the $n = 5$ resonance ($\Delta t \approx 2.9$ fs). Both planar and three-dimensional views are shown. The black, dotted line in the planar view corresponds to the analytical solution. The different colors distinguish maps at different timesteps. Starting with $\Delta t = 2.9190$ fs (purple-blue), the timestep is incremented by 0.0005 fs, up to $\Delta t = 2.9230$ fs (red). Clearly, the phase space is disconnected near this resonance, revealing five islands

What is evident from these views is that separate, discontinuous regions (islands) are spanned by trajectories near this timestep.

The pentagonal/oval shape of the diagrams in Fig. 3 and the five-island pattern suggests a resonance of order five [25]. Similarly, the four islands of Fig. 2c ($\Delta t = 4.02$ fs) indicate a resonance of order four. The triangular shapes associated with the trajectories of Figs. 2d and 2e ($\Delta t = 6.7, 7.22$ fs), as well as the instability occurring in this range of timestep (Fig. 1), point to a resonance of order three [25]. The origin of these resonances is discussed in more detail below.

4. Discussion

It is known that any symplectic integration scheme applied to a nonlinear autonomous system with Hamiltonian $H(X, V)$ is equivalent to the exact sampling of some perturbed, nonautonomous system with an effective Hamiltonian $H_{\text{eff}}(X, V, \Delta t)$, where

$$H_{\text{eff}}(X, V, \Delta t) = H(x) + \mathcal{O}((\Delta t)^{\beta}), \tag{13}$$

with β denoting the order of the integration scheme [12]. Recently, Wang proved that this effective Hamiltonian is time-periodic with period Δt [18]. Thus, trajectories generated by a symplectic algorithm correspond to some Hamiltonian that depends periodically on the timestep. In such a system resonance can occur when a special relationship holds between the forcing frequency ($2\pi/\Delta t$) and the frequency of the periodic motion, ω [25]. For our Morse oscillator system the resonance condition the takes form

$$n\omega = m\frac{2\pi}{\Delta t}, \tag{14}$$

where n and m are relatively prime natural numbers and n is known as the *order* of the resonance.

It is well known that IM affects the frequency of the periodic motion of the system [26]. The effective frequency, ω^{eff}, becomes timestep dependent. The exact analytical formula for ω^{eff} of our nonlinear Morse oscillator system is not known, but for relatively small energy values it is reasonable to approximate this effective frequency by expressions known for harmonic oscillators.

For a one-dimensional harmonic oscillator of natural angular frequency ω_0, the IM propagation of the position, x, and velocity, v, corresponds to the following rotation in $(v, \omega_0 x)$ space [26]:

$$\begin{pmatrix} v^{n+1} \\ \omega_0 x^{n+1} \end{pmatrix} = \begin{pmatrix} \cos\theta & -\sin\theta \\ \sin\theta & \cos\theta \end{pmatrix} \begin{pmatrix} v^{n} \\ \omega_0 x^{n} \end{pmatrix}. \tag{15}$$

The angle of rotation, θ, a function of the timestep, is given by the formula

$$\theta = 2\tan^{-1}(\tfrac{1}{2}\omega_0 \Delta t), \tag{16}$$

or equivalently,

$$\theta = \tan^{-1}\left(\frac{\omega_0 \Delta t}{1 - \frac{1}{4}(\omega_0 \Delta t)^2}\right). \quad (17)$$

Thus, θ depends on the timestep in a nonlinear way. The discretized motion of the harmonic oscillator occurs with a modified, *effective* angular frequency, ω_0^{eff}, defined as

$$\omega_0^{\text{eff}} = \frac{\theta}{\Delta t} = \frac{2}{\Delta t}\tan^{-1}(\tfrac{1}{2}\omega_0 \Delta t). \quad (18)$$

The effective period, T_0^{eff}, is then given by

$$T_0^{\text{eff}} = \frac{\pi \Delta t}{\tan^{-1}(\frac{1}{2}\omega_0 \Delta t)}. \quad (19)$$

Note that as $\Delta t \to 0$, $\omega_0^{\text{eff}} \to \omega_0$, and as $\Delta t \to \infty$, $\omega_0^{\text{eff}} \to \pi/\Delta t = 0$.

A plot of effective angular frequency, ω_0^{eff}, for three different values of the original angular frequency of the harmonic oscillator, ω_0 ($\omega_0 = 1, 2$ and 3 rad) is shown in Fig. 1d. We note that ω_0^{eff} is close to ω_0 only for very small values of the timestep Δt. For intermediate values of Δt the curves sharply decay, converging slowly to zero. This monotonic decrease of ω_0^{eff} with the timestep explains our observation of a series of resonances of different order. Note also that different natural frequencies are mapped onto *one* effective frequency in the limit of large timesteps. This suggests a troubling scenario for biomolecules, whose motions are made possible by a large range of *different*, but cooperative, characteristic motions.

Inserting Eq. (18) into the resonance condition (Eq. (14)) and solving for Δt we get the approximate formula for timesteps, $\Delta t_{n,m}$, at which resonances of order n occur,

$$\Delta t_{n,m} = \frac{2}{\omega_{E_i^0}} \tan\left(\frac{m\pi}{n}\right), \quad \frac{n}{m} > 2. \quad (20)$$

(At those timesteps, the harmonic oscillator samples exactly n phase space points in m revolutions, where $n\theta = n\Delta t \omega^{\text{eff}} = m\,2\pi$.)

For our Morse system, the predicted timesteps with $m = 1$, corresponding to the lowest-order resonances, are presented in Table 1. The agreement between the predicted (Table 1) and observed resonance timesteps (Figs. 1a–1c) is very good.

Table 1
The predicted timesteps, $\Delta t_{n,1}$ (fs), for resonance of the Morse oscillator system. The variable n denotes the resonance order and $\Delta t_{n,1}$ is computed according to Eq. (20) with $\omega_{E_i^0} = 0.497$ fs^{-1}. The third column gives $\Delta t_{n,1}$ in period units ($T_{E_i^0} = 12.6$ fs). Only the six lowest-order resonances are listed

n	$\Delta t_{n,1}$	Period fraction
3	6.97	0.55
4	4.02	0.32
5	2.91	0.23
6	2.32	0.18
7	1.94	0.15
8	1.67	0.13

From the data in Table 1, we expect for $\Delta t = 2$ fs to observe resonance of order $n = 7$ for relatively low energies. In fact, from Eq. (20) we can estimate the minimum value of $\frac{n}{m}$ for feasible resonances at given timestep. For $\Delta t = 2$ fs this value is close to 6.8. Indeed, this agrees with the pattern of seven islands seen in Fig. 4a. With increasing values of energy, and thus the corresponding period of the system, a systematic emergence of higher-order resonances ($\frac{n}{m} = \frac{8}{1}, \frac{9}{1}$ and $\frac{29}{3}$) is evident. For comparison with IM, the phase space portrait obtained with leap-frog at $\Delta t = 2$ fs is presented in Fig. 4b. Resonances are expected, since leap-frog is also symplectic [23]. The relationship between the timestep and the order of the resonance is different though: in leap-frog, the angle of rotation in phase space, $\theta(\Delta t)$, is different than in IM [27]. At the same timestep ($\Delta t = 2$ fs), resonances of different order are observed in both schemes. In Fig. 4b, the resonance of order $n = 6$ is seen for small values of energy and resonances of increasing ratio $\frac{n}{m}$ ($\frac{13}{2}, \frac{20}{3}$) occur as the energy increases.

Fig. 5 illustrates the severity of the third-order resonance: the stability region is decreased around the equilibrium point of our Morse oscillator system as the resonant timestep $\Delta t_{3,1}$ is approached (note diverging patterns). This was predicted by Arnold [25]. The case of $n = 4$ (around $\Delta t = 4.02$ fs here) leads to large energy fluctuations but not instability in IM (instability can result from other integrators and systems [25]). In agreement with Arnold, we do not observe instability for resonances of order higher than four [25]. In particular, the resonances of order higher than $n = 5$ do not cause large energy fluctuations but

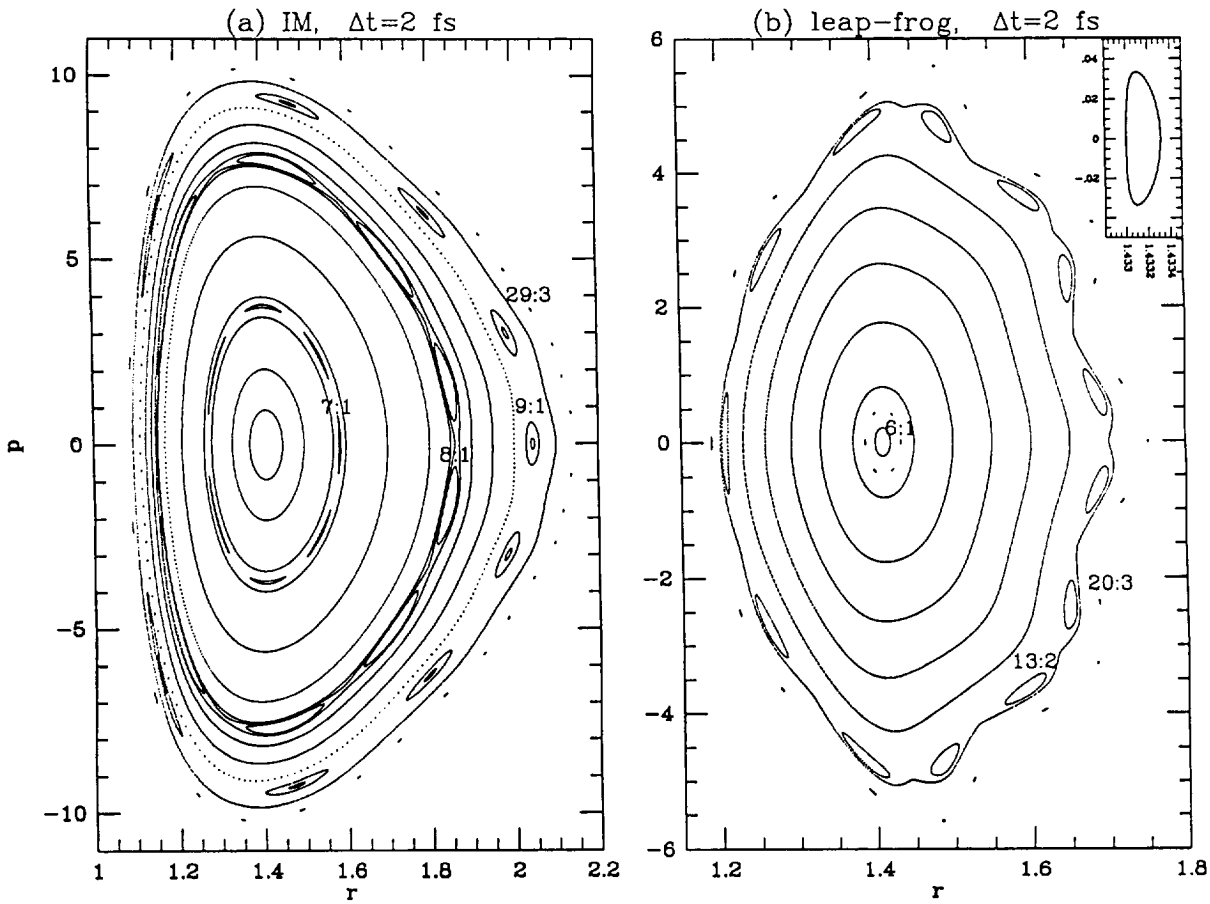

Fig. 4. Phase diagrams at a fixed timestep, Δt = 2.0 fs, with (a) IM and (b) leap-frog. Initial conditions are chosen by changing the initial position and keeping the initial momentum zero. Plots show creations of resonances of different orders. In plot (a) the resonances n = 7, 8 and 9 are clearly seen. Also the 29 islands of the resonance 29/3 are present. In plot (b) the resonance n = 6 is seen. (The inset shows one of the associated islands of that resonance in an enlarged scale; to complete the loop it was necessary to use trajectory of 50000 points.) The other resonances shown are of higher order, 13/2 and 20/3. In both cases, as the initial energy increases, the resonance order increases.

their presence can be detected by the islands created in the phase diagrams.

The existence of periodic perturbation for any timestep means that the resonances will occur even for very small timesteps ($\Delta t \ll T_{E_i}$). For small timesteps, however, the energy fluctuations are not as significant as those associated with lower-order resonances. Still, for large systems the discretization-induced perturbation (Eq. (13)) might lead to resonances that exhibit 'diffusion' in phase space (Arnold diffusion [28]), i.e. sampling of regions that the unperturbed system would not. Although that process might increase the ergodicity of sampling, the resulting trajectory should not be viewed as deterministic. The generated *successive* snapshots of the system may bear little resemblance to the dynamics of the original system.

In the large timestep limit, however, the effect of the discretization – nonlinear change of frequencies of the system as well as linearization of the system – might not reproduce expected behavior and also lead to effects not seen in the original system.

5. Conclusions

We have studied the problem of resonance by an implicit symplectic integrator, IM, for a nonlinear chem-

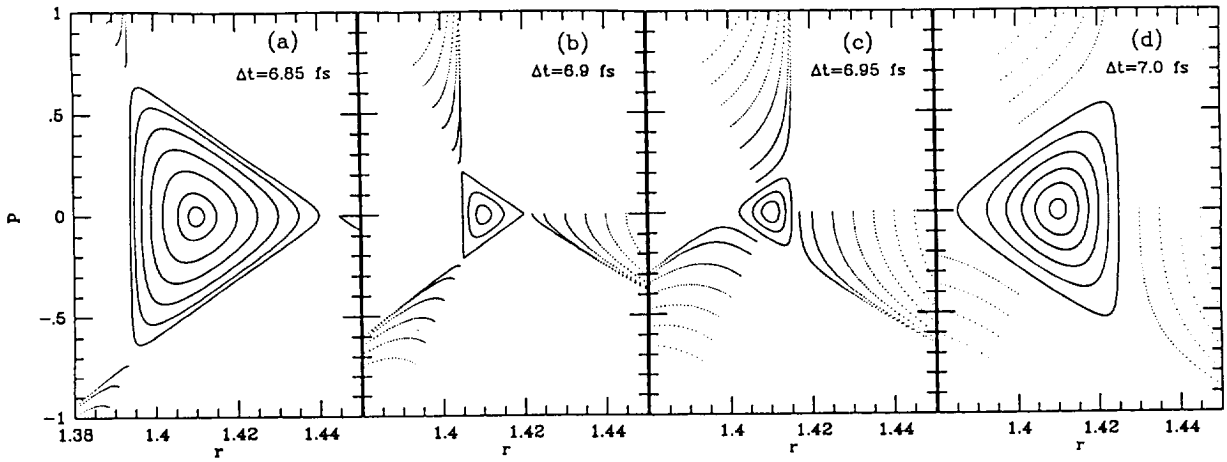

Fig. 5. Phase diagrams at different timesteps near the resonance $n = 3$. For each timestep, different initial conditions are chosen to show the decrease of the stability region as the order $n = 3$ resonance ($\Delta t = 6.97$ fs) is approached.

ical system. Relatively large timesteps were examined to understand the differences between the systematic and erratic errors. We showed how the dynamics can be corrupted at and/or near resonant timesteps and how these problems can be detected. By relying on the large body of knowledge in the classical mechanics literature, we have presented an analysis that leads to prediction of the timesteps where the resonances should occur (Eq. (20)). This analysis is confirmed by our simulation results (Figs. 1a–1c, 2c–2e, 3–5). In sum, the following conclusions can be drawn regarding the IM integrator.

(1) For small Δt, IM is better than leap-frog in terms of energy fluctuations. As seen in Fig. 1c, IM errors at $\Delta t = 2$ fs (roughly one sixth of the period) are smaller than those of leap-frog for $\Delta t = 1$ fs by a factor of 2.5. Still, the computational time of IM is probably not competitive.

(2) For large timesteps ($\Delta t > 10$ fs), energy fluctuations are bound but the force is effectively linearized and the frequency severely damped. See Fig. 1a and the phase diagram of Fig. 2f, as well as Eq. (18) and Fig. 1d.

(3) Resonance problems are expected for the Morse oscillator according to Eq. (13). Here we observe resonances of order $n = 3, 4, 5$ ($m = 1$) (see Figs. 1a–1c, 2c–2e and 3), corresponding to $\Delta t = 6.97, 4.02, 2.91$ fs (roughly one half, one third, and one fourth the period), respectively. Higher-order resonances, $n = 7, 8, 9$ with $m = 1$ (Δt smaller than roughly one seventh of the period), are seen in Fig. 4a. Also, the resonance $\frac{n}{m} = \frac{29}{3}$ is evident in Fig. 4a. However, we found that only the lowest-order resonance, namely $n = 3$ and $m = 1$ ($\Delta t = 6.97$), leads to instability (Figs. 1a and 5). In severity, the resonance of order $n = 4$ follows $n = 3$ ($m = 1$). Beyond $n = 5$, resonances can only be detected in the phase diagrams (Fig. 4), not by the energy fluctuations, which are small. (The resonances displayed in this work do not of course exhaust all the possible cases.)

(4) For biomolecules, resonance problems are expected to affect the dynamics severely at moderate and large timesteps. Thus, extreme caution must be exercised in this regime when symplectic methods are used. Although systematic errors due to the discretization scheme are expected when the timestep is relatively large with respect to the period of the fastest motion, we have shown here how additional, erratic problems due to resonance can occur for symplectic methods. We emphasize that our analysis does not rule out resonance in non-symplectic schemes. Not only are timestep-dependent resonances expected, but also *artificial coupling* of motion associated with different frequencies due to their nonlinear mapping (Fig. 1d). Based on the harmonic oscillator analysis, we expect that at large timesteps all the high frequencies of the system are effectively mapped to one frequency, approaching zero at large Δt (Eq. (18), Fig. 1d). Moreover, in this timestep regime, the forces governing the fast motions are effectively linearized (Fig. 2f), so the

resulting dynamics may be unrealistic. An application of IM to a more complex molecular system, to explore these intriguing observations and scenarios, and possibly devise a remedy, is underway.

Acknowledgement

We thank Sebastian Reich and Bob Skeel for pointing us to interesting references. This research was generously supported by the National Science Foundation (CHE-9002146, PYI Award ASC-915782, and GCAG ASC-9318159), the National Institutes of Health (Research Resource RR08102), the Alfred Sloan Foundation and the Howard Hughes Medical Institute.

References

[1] J.A. McCammon and S.C. Harvey, Dynamics of proteins and nucleic acids (Cambridge Univ. Press, Cambridge, 1987).
[2] T. Schlick, in: Program proceedings, IMA volumes in mathematic and its applications, eds. J. Mesirov and K. Schulten (Springer, Berlin, 1994), in press.
[3] G. Zhang and T. Schlick, J. Comput. Chem. 42 (1993) 1212.
[4] J.D. Lambert, Numerical methods for ordinary differential systems (Wiley, New York, 1991).
[5] C.S. Peskin and T. Schlick, Commun. Pure. Appl. Math. 42 (1989) 1001.
[6] T. Schlick and C.S. Peskin, Commun. Pure. Appl. Math. 42 (1989) 1141.
[7] G. Zhang and T. Schlick, J. Chem. Phys. 101 (1994) 4995.
[8] T. Schlick and W. Olson, J. Mol. Biol. 223 (1992) 1089.
[9] G. Ramachandran and T. Schlick, Phys. Rev. E, submitted for publication.
[10] A. Nyberg and T. Schlick, Chem. Phys. Letters 198 (1992) 538.
[11] P.J. Channel and C. Scovel, Nonlinearity 3 (1990) 231.
[12] J.M. Sanz-Serna and M.P. Calvo, Numerical Hamiltonian problems (Chapman and Hall, London, 1994).
[13] S.K. Gray and D.W. Noid and B.G. Sumpter, J. Chem. Phys. 101 (1994) 4062.
[14] Feng Kang, in: Applied and industrial mathematics, ed. R. Spigler (Kluwer, Dordrecht, 1990) p. 17.
[15] J.C. Simo, N. Tarnow and K.K. Wong, Comput. Meth. Appl. Mech. Eng. 100 (1992) 63.
[16] J.C. Simo and N. Tarnow, ZAMP 43 (1992) 757.
[17] O. Gonzales and J.C. Simo, preprint.
[18] D. Wang, Physica D 73 (1994) 1.
[19] T. Schlick and A. Fogelson, ACM transactions on mathematical software 18 (1992) 46.
[20] T. Schlick and A. Fogelson, ACM transactions on mathematical software 18 (1992) 71.
[21] L. Verlet, Phys. Rev. 159 (1967) 98.
[22] M.P. Allen and D.J. Tildesley, Computer simulations of liquids (Claredon Press, Oxford, 1987).
[23] D.I. Okunbor and R.D. Skeel, J. Comput. Chem. 15 (1994) 72.
[24] N.B. Slater, Nature 180 (1957) 1352.
[25] V.I. Arnold, Mathematical methods of classical mechanics (Springer, Berlin, 1989)
[26] G. Zhang and T. Schlick, Mol. Phys., in press.
[27] R.D. Skeel, BIT 33 (1993) 172.
[28] M.A. Lieberman, in: Nonlinear dynamics, ed. R.H.G. Helleman (New York Academy of Sciences, New York, 1980) p. 119.